A&A 547, A10 (2012)
DOI: 10.1051/0004-6361/201219396

Astronomy & Astrophysics

Analysis of the rotation period of asteroids (1865) Cerberus, (2100) Ra-Shalom, and (3103) Eger – search for the YORP effect⋆

J. Ďurech[1], D. Vokrouhlický[1], A. R. Baransky[2], S. Breiter[3], O. A. Burkhonov[4], W. Cooney[5], V. Fuller[6], N. M. Gaftonyuk[7], J. Gross[5], R. Ya. Inasaridze[8], M. Kaasalainen[9], Yu. N. Krugly[10], O. I. Kvaratshelia[8], E. A. Litvinenko[11], B. Macomber[12], F. Marchis[12,13], I. E. Molotov[14], J. Oey[15], D. Polishook[16], J. Pollock[6], P. Pravec[17], K. Sárneczky[18], V. G. Shevchenko[7], I. Slyusarev[7] R. Stephens[19], Gy. Szabó[18,20,23], D. Terrell[5], F. Vachier[21], Z. Vanderplate[6], M. Viikinkoski[9], and B. D. Warner[22]

[1] Astronomical Institute, Faculty of Mathematics and Physics, Charles University, V Holešovičkách 2, 18000 Prague, Czech Republic
e-mail: durech@sirrah.troja.mff.cuni.cz
[2] Astronomical Observatory of Taras Shevshenko National University, Astronomichna str. 3, Kiev, Ukraine
[3] Astronomical Observatory Institute, Faculty of Physics, Adam Mickiewicz University, Słoneczna 36, 60-286 Poznań, Poland
[4] Ulugh Beg Astronomical Institute, Uzbek Academy of Sciences, Astronomicheskaya 33, Tashkent 100052, Uzbekistan
[5] Sonoita Research Observatory, 1442 E Roger Rd, Tuscon, AZ 85719, USA
[6] Physics and Astronomy Department, Appalachian State University, Boone, NC 28608, USA
[7] Crimean Astrophysical Observatory, Simeiz Department, Simeiz 98680, Ukraine
[8] Kharadze Abastumani Astrophysical Observatory, Ilia State University, G.Tsereteli str. 3, Tbilisi 0162, Georgia
[9] Department of Mathematics, Tampere University of Technology, PO Box 553, 33101 Tampere, Finland
[10] Institute of Astronomy of Kharkiv National University, Sumska str. 35, Kharkiv 61022, Ukraine
[11] The Central (Pulkovo) Astronomical Observatory of the Russian Academy of Sciences, Pulkovskoye chaussee 65/1, St.-Petersburg 196140, Russia
[12] University of California at Berkeley, Department of Astronomy, 601 Campbell Hall, Berkeley, CA 94720, USA
[13] Carl Sagan Center, SETI institute, 189 Bernardo Av., Mountain View CA 94043, USA
[14] Keldysh Institute of Applied Mathematics, RAS, Miusskaya sq. 4, 125047 Moscow, Russia
[15] Kingsgrove Observatory, 23 Monaro Ave., Kingsgrove, NSW, Australia
[16] Department of Earth, Atmospheric, and Planetary Sciences, Massachusetts Institute of Technology, Cambridge, MA 02139, USA
[17] Ondřejov Observatory, AV ČR, 251 65 Ondřejov, Czech Republic
[18] Konkoly Observatory of the Hungarian Academy of Sciences, PO Box 67, 1525 Budapest, Hungary
[19] Goat Mountain Astronomical Research Station, 11355 Mount Johnson Court, Rancho Cucamonga, CA 91737, USA
[20] Department of Experimental Physics, University of Szeged, Dóm tér 9, 6720 Szeged, Hungary
[21] Institut de Mécanique Céleste et de Calcul des Éphémérides, Observatoire de Paris, UMR8028 CNRS, 77 Av. Denfert-Rochereau, 75014 Paris, France
[22] Palmer Divide Observatory, 17955 Bakers Farm Rd., Colorado Springs, CO 80908, USA
[23] ELTE Gao-Lendület Research Group, 9700 Szombathely, Hungary

Received 12 April 2012 / Accepted 5 September 2012

ABSTRACT

Context. The spin state of small asteroids can change on a long timescale by the Yarkovsky-O'Keefe-Radzievskii-Paddack (YORP) effect, the net torque that arises from anisotropically scattered sunlight and proper thermal radiation from an irregularly-shaped asteroid. The secular change in the rotation period caused by the YORP effect can be detected by analysis of asteroid photometric lightcurves.

Aims. We analyzed photometric lightcurves of near-Earth asteroids (1865) Cerberus, (2100) Ra-Shalom, and (3103) Eger with the aim to detect possible deviations from the constant rotation caused by the YORP effect.

Methods. We carried out new photometric observations of the three asteroids, combined the new lightcurves with archived data, and used the lightcurve inversion method to model the asteroid shape, pole direction, and rotation rate. The YORP effect was modeled as a linear change in the rotation rate in time $\mathrm{d}\omega/\mathrm{d}t$. Values of $\mathrm{d}\omega/\mathrm{d}t$ derived from observations were compared with the values predicted by theory.

Results. We derived physical models for all three asteroids. We had to model Eger as a nonconvex body because the convex model failed to fit the lightcurves observed at high phase angles. We probably detected the acceleration of the rotation rate of Eger $\mathrm{d}\omega/\mathrm{d}t = (1.4 \pm 0.6) \times 10^{-8}\,\mathrm{rad\,d^{-2}}$ (3σ error), which corresponds to a decrease in the rotation period by $4.2\,\mathrm{ms\,yr^{-1}}$. The photometry of Cerberus and Ra-Shalom was consistent with a constant-period model, and no secular change in the spin rate was detected. We could only constrain maximum values of $|\mathrm{d}\omega/\mathrm{d}t| < 8 \times 10^{-9}\,\mathrm{rad\,d^{-2}}$ for Cerberus, and $|\mathrm{d}\omega/\mathrm{d}t| < 3 \times 10^{-8}\,\mathrm{rad\,d^{-2}}$ for Ra-Shalom.

Key words. minor planets, asteroids: individual: (1865) Cerberus – minor planets, asteroids: individual: (2100) Ra-Shalom – minor planets, asteroids: individual: (3103) Eger – methods: data analysis – techniques: photometric

⋆ Tables 1–3 are available in electronic form at
http://www.aanda.org

1. Introduction

The anisotropic reflection of sunlight and thermal emission of an asteroid results in a net torque that modifies the asteroid's spin state in the long term. This effect, called Yarkovsky-O'Keefe-Radzievskii-Paddack (YORP), is important for the spin-state evolution of asteroids in the size range from ~1 m to ~40 km (Bottke et al. 2006). In particular, YORP can reorient the asteroid's spin axis, slow down or spin up their rotation, and trigger a tumbling state. YORP has been found to be a key element in understanding the peculiar rotation pole distribution of large Koronis-family members (Vokrouhlický et al. 2003), the distribution of small members in moderately young asteroid families (Vokrouhlický et al. 2006), and the distribution of the rotation rate of small main-belt asteroids (Pravec et al. 2008; Polishook & Brosch 2009). Thanks to its ability to bring asteroid rotation toward the fission limit, it has been suggested that it is a universal formation mechanism for small binary asteroids (Scheeres 2007; Pravec & Harris 2007; Walsh et al. 2008) and asteroid pairs (Vokrouhlický & Nesvorný 2008; Pravec et al. 2010). Although the importance of YORP is now widely recognized, the YORP effect has been detected on only three asteroids so far: (1862) Apollo (Kaasalainen et al. 2007), (54509) YORP (Lowry et al. 2007; Taylor et al. 2007), and (1620) Geographos (Ďurech et al. 2008). Here we extend this list with a new YORP detection for asteroid (3103) Eger.

The primary importance of YORP detection for specific bodies consists in the possibility of validating the theoretical modeling of YORP itself. This is especially important after several studies have demonstrated possible difficulties in the theoretical prediction of the YORP effect magnitude, such as a non-uniform distribution of density (Scheeres & Gaskell 2008), a sensitive dependence on small-scale irregularities in the shape (Statler 2009; Breiter et al. 2009) and the degree of thermal beaming (Rozitis & Green 2012). As a result, some cases of nondetections might be as important as the positive detections (Scheeres & Gaskell 2008; Breiter et al. 2009). These are the cases where the simple YORP theory predicts a possible detection for a present data set, yet an accurate analysis of the observations does not reveal any sign of it.

Motivated by the discussion above, we present new photometric observations of near-Earth asteroids (1865) Cerberus, (2100) Ra-Shalom, and (3108) Eger. We derived a shape model and spin state for these asteroids and detected the acceleration of the rotation rate of Eger, which we believe is produced by the YORP effect[1]. For the two other asteroids we studied – (1865) Cerberus and (2100) Ra-Shalom – we set only upper limits on the change in the rotation rate. While in the Ra-Shalom case this observational bound is about the upper limit of the expected theoretical YORP value for a body of its size and heliocentric orbit, in the case of Cerberus, the constraint is much stronger. Reminiscent of the case of (25143) Itokawa, the expected Cerberus YORP value is a factor of ~3 higher than its observed limit.

2. Lightcurve inversion and search for the rotation-period change

We used the lightcurve inversion method of Kaasalainen & Torppa (2001) and Kaasalainen et al. (2001) to derive asteroids' shape, sidereal rotation period, and spin axis direction from the observed lightcurves. Following the method of Kaasalainen et al. (2003), we assumed that the rotation rate ω changes linearly with time as $\omega(t) = \omega_0 + \upsilon t$. Both ω_0 and $\upsilon \equiv \mathrm{d}\omega/\mathrm{d}t$ were free parameters of the optimization. We analyzed the difference (measured by the χ^2 values of the goodness-of-fit) between a constant-period model ($\upsilon = 0$) and a model with $\upsilon \neq 0$. If this difference is small, the data can be fitted with the constant-period model and no deviation from the uniform rotation is detected. If, on the other hand, the fit for $\upsilon \neq 0$ is significantly better than for $\upsilon = 0$, the change in the rotation rate is detected.

We found a significant change in the rotation period only for asteroid Eger. For Cerberus and Ra-Shalom, the constant-period model fitted the available data well, and the free parameter υ did not improve the fit significantly. To estimate the maximum value of $|\mathrm{d}\omega/\mathrm{d}t|$ that still agrees with observations, we increased or decreased υ and found the value of χ^2, for which the discrepancy between the data and the model became significant.

2.1. (3103) Eger

Kaasalainen et al. (2002) have derived a preliminary shape model of Eger from 13 lightcurves observed between 1986 and 1997. These lightcurves were obtained by Wisniewski (1987), Wisniewski (1991), Velichko et al. (1992), de Sanctis et al. (1994), and Pravec et al. (1998). The data were archived in the Uppsala Asteroid Photometric Catalog (UAPC) (Lagerkvist et al. 2001). We observed Eger during its seven apparitions between 1997 and 2012. The aspect data for these new photometric observations are listed in Table 1. A detailed description of the reduction and measurement procedures at the Wise Observatory can be found in Polishook & Brosch (2008). CCD observations and data processing at Kharkiv, Simeiz, Maidanak, Lisnyky, and Kitab observatories were done in the standard way, and the details can be found in Krugly et al. (2002). It is particularly important that during three apparitions – 1997, 2007, and 2009 – our observations were not taken at the Earth close encounters of Eger, thus providing data at new viewing geometries. This is because Eger is presently close to the 3/5 exterior mean motion resonance with the Earth (Milani et al. 1989), and so the viewing geometry at close approaches repeats.

The photometric data set consists of 70 lightcurves covering more than twenty years. Some of them were observed at unusually high phase angles larger than 75 deg. The usual approach of lightcurve inversion – using the convex shape model, together with the combination of Lommel-Seeliger and Lambert scattering laws – did not succeed in fitting these high-phase lightcurves. The large discrepancy between the data and the model was an indication of a significant nonconvexity of the shape of Eger (Ďurech & Kaasalainen 2003). When we used Hapke's scattering model, the fit improved but was still not good. However, we obtained a good fit when modeling the shape of Eger as a general nonconvex body using the approach of Kaasalainen & Viikinkoski (2012).

We derived a unique solution for the sidereal rotation period P, the change in the rotation rate υ, the pole direction λ, β in ecliptic coordinates, and the shape. The best-fit parameters are as follows: $\lambda = 226° \pm 15°$, $\beta = -70° \pm 4°$, $P = 5.710156 \pm 0.000007$ h (for JD 2446617.0), and $\upsilon = (1.4 \pm 0.6) \times 10^{-8}$ rad d^{-2}. These parameters and their uncertainties were derived using the weights of individual lightcurves that corresponded to the inverse of the noise. When all lightcurves have the same weight regardless of their quality, the formal

[1] The whole lightcurve dataset, shape model parameters, and other details are available from the DAMIT website http://astro.troja.mff.cuni.cz/projects/asteroids3D (see also Ďurech et al. 2010).

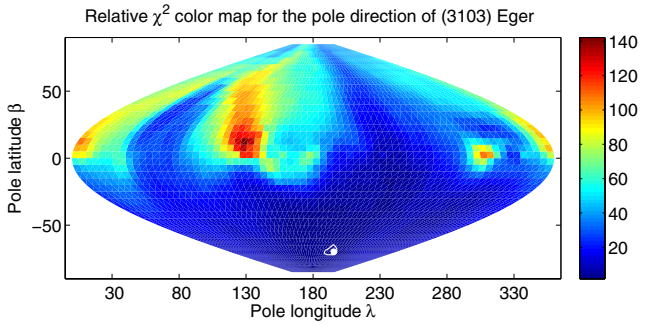

Fig. 1. Statistical quality of Eger pole solutions given in sinusoidal projection of the sky in ecliptic coordinates. The grade of shading and the scale bar on the right indicate the χ^2 of the fit divided by the number of data points. The formally best-fit case with $\lambda = 226°$ and $\beta = -70°$ is marked with a full circle. The solid line shows the contour with the χ^2 value 6% higher than the minimum value of the best-fit solution. It represents our region of admissible solutions.

best-fit value of υ is 1.2×10^{-8} rad d^{-2}. The fit to the lightcurves for $\upsilon = 0$ is very good with only small phase shifts between the model and the data. However, using nonzero values for the υ parameter improves the fit significantly. The uncertainty intervals were estimated from the increase in χ^2 when varying the model parameters. The reported errors correspond to 3σ for the χ^2 distribution with ~4700 degrees of freedom[2]. Although the relative uncertainty of υ is large, the zero value is outside the formal uncertainty interval. For $\upsilon = 0$, the fit is significantly worse (30% higher χ^2) than for the best model. We also note that the angular difference of ~55° between our solution and the best-fit solution by Kaasalainen et al. (2002) is significant and arises from the limited number of lightcurves used to derive the previous model. The pole direction is very well constrained and is not sensitive to the value of υ, the scattering model, or the shape parametrization. The 3σ uncertainty region is shown in Fig. 1.

As an additional check of consistency, we note that our pole solution closely matches a constraint that was suggested from the 1991 and 1996 radar observations (Benner et al. 1997). In particular, the viewing geometry at the end of July 1996 was nearly equatorial for our pole as suggested by this reference. In 1991 Aug. 10, the line of sight was indeed closer to the pole by ~15°.

The shape model of Eger is shown in Fig. 2. Although some of the lightcurves (those published by Pravec et al. 1998) were accurately calibrated to standard R or V magnitudes, they did not cover the viewing/illumination geometry sufficiently to use them for constraining the model. Therefore, we treated all the calibrated lightcurves as relative.

In general, nonconvex models are much less stable than convex ones with respect to the errors in the data, the level of regularization, the scattering model, etc. However, this is the first time the nonconvex shape fits the lightcurves that were observed at large phase angles significantly better than the convex one. The nonconvex model in Fig. 2 is only one of many similar models that we obtained using different regularization, scattering models, and resolution. Apparently, the model contains many details that may lead to misinterpretation. The main concavity is likely to be real because it repeats for models with different regularization. The other details differ from model to model and are instead artifacts of the modeling process.

[2] The χ^2 distribution with ν degrees of freedom has mean ν and variance 2ν. For Eger, the number of data points was ≃4800, the number of model parameters ≃100, thus the number of degrees of freedom was $\nu \simeq 4700$.

The lightcurve fits for models with $\upsilon = 0$ and $\upsilon \neq 0$ are shown in Fig. 3. The difference between the two models is clearly visible only for lightcurves from 1986, 1987, and 1996. Because both the number of lightcurves and the number of data points in the lightcurves increase towards more recent observations, there is almost no phase shift between the models for observations between 2006–2012. The sign of the phase shift is different for different epochs.

This is further demonstrated in Fig. 4, where the shift in phase between the observed and modeled lighcurves is plotted. Although the scatter in the phase shifts is of minutes, there is a clear quadratic trend for the constant period model (top panel), which is what we expect if the rotation rate changes linearly in time. The best-fit quadratic function corresponds to $\upsilon = 0.8 \times 10^{-8}$ rad d^{-2}. This is different from the value obtained by the lightcurve inversion, because with lightcurve inversion, the difference between the observed and modeled brightness is minimized, not the phase shift between the observed and modeled lightcurves. In the bottom panel, the phase differencies are plotted for the YORP model with $\upsilon = 1.2 \times 10^{-8}$ rad d^{-2} (equal weights for all lightcurves). For this value of υ, there is no quadratic trend, and the points are randomly distributed along the zero value.

However, the period analysis depends critically on the observations from 1986/87 and is very sensitive to possible systematic errors. Although the data came from three different works (Wisniewski 1987, 1991; de Sanctis et al. 1994), which should largely eliminate any possible observational errors, there is an insufficient check against potential systematic model errors. Therefore, our detection of the acceleration of Eger's rotation due to YORP appears plausible, but it will have to be nailed down with more observations in upcoming apparitions (2014, 2016, 2017, 2019, etc.) so that it becomes a robust detection. With more observations, the time line will be enlarged and the quadratic trend seen in Fig. 4 can be confirmed.

2.2. (1865) Cerberus

Cerberus lightcurves are characterized by unusually large amplitude, up to 2.3 mag, which is the largest lightcurve amplitude observed so far for any asteroid. The UAPC contains the photometry of Cerberus from 1980 (Harris & Young 1989), 1989 (Wisniewski et al. 1997), and 1998 (Sárneczky et al. 1999), while additional photometric observations were published by Szabó et al. (2001). Until now, any pole solution had not been determined. We observed Cerberus during three apparitions in 1999, 2008, and 2009. The circumstances of these observations are listed in Table 2.

We derived a physical model of Cerberus with the sidereal rotation period $P = 6.80328 \pm 0.00001$ h and the pole direction $\lambda = 298° \pm 40°$, $\beta = -72° \pm 10°$. The pole direction is well constrained, and the 3σ uncertainty region is shown in Fig. 7. The convex shape model (Fig. 5) is very elongated with semiaxis ratios $a/c \simeq 4.5$ and $b/c \simeq 1.5$, suggesting that the real shape of Cerberus might be bilobed or even consist of a close synchronous binary. When using calibrated lightcurves, the model is even more elongated and flat with $a/c \sim 7$ and $b/c \sim 2$. The constant-period model fits well with all available lightcurves. Introducing the $\upsilon \neq 0$ parameter into the modeling did not improve the fit. We estimated the maximum allowed absolute value of the period change to be $|\upsilon| < 8 \times 10^{-9}$ rad d^{-2}. If the change in the rotation rate were higher, it would be detectable in the lightcurve set as a shift between observations and the model of about 10°.

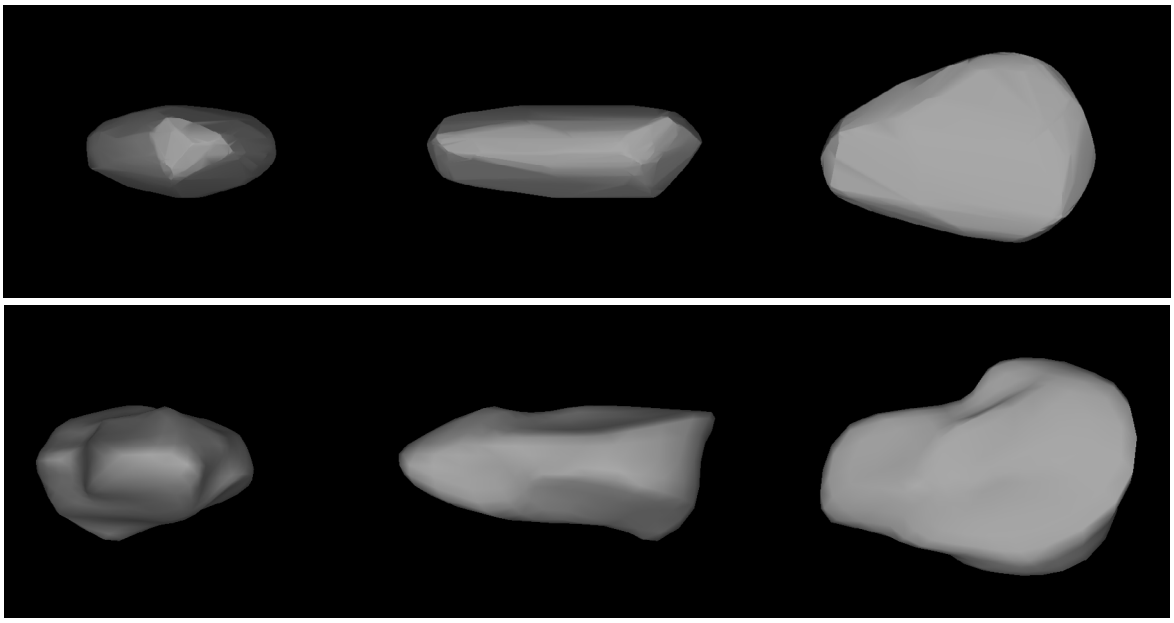

Fig. 2. Convex (*top*) and nonconvex (*bottom*) shape models of Eger shown from equatorial level (*left, center*) and pole-on (*right*).

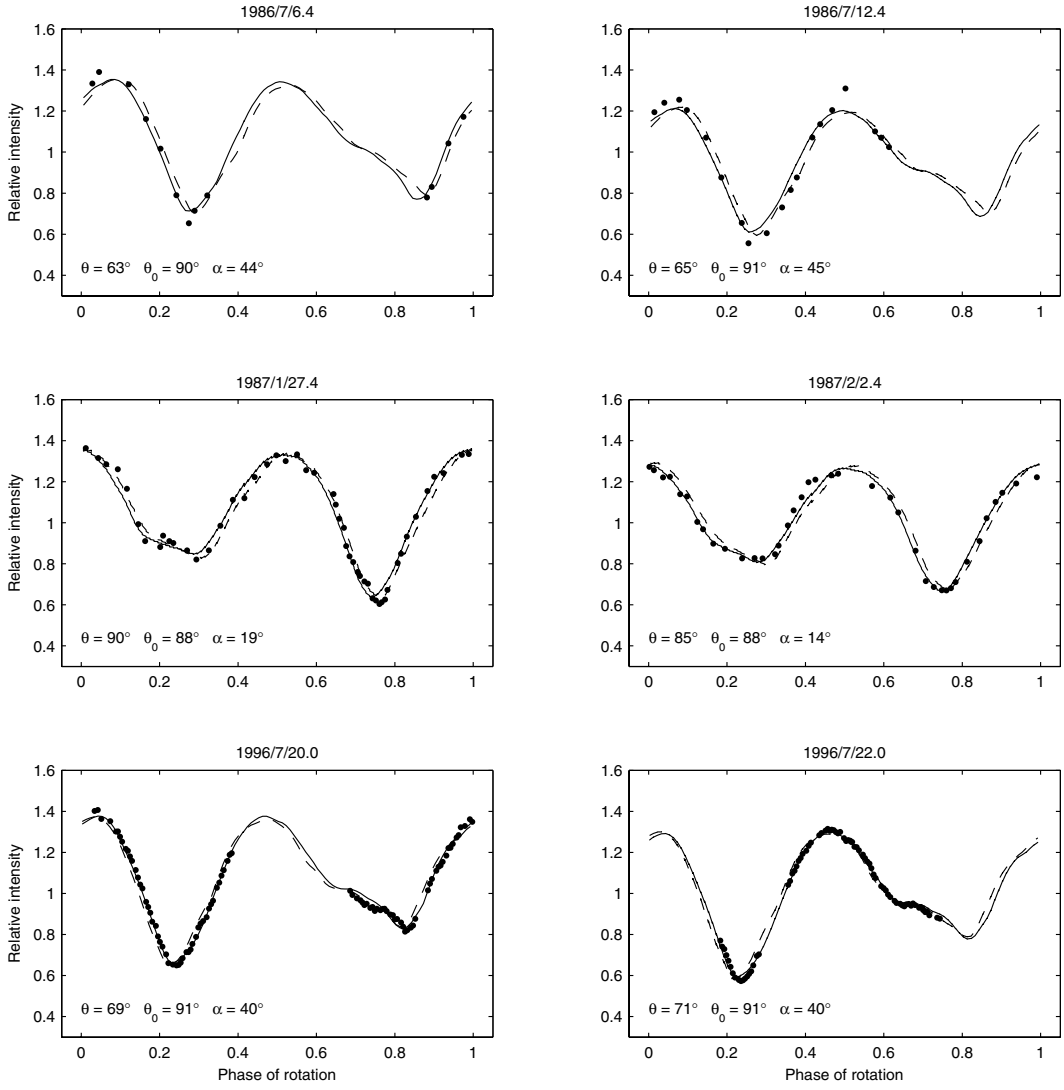

Fig. 3. Examples of Eger's photometric data (points) fitted with synthetic lightcurves based on the convex shape model. The solid curve corresponds to the best model with the rotation rate accelerated by $\upsilon = 1.2 \times 10^{-8}$ rad d^{-2}, while the dashed curve corresponds to the best constant-period model with $\upsilon = 0$. The viewing and illumination geometry is given by the aspect angle θ, the solar aspect angle θ_0, and the solar phase angle α.

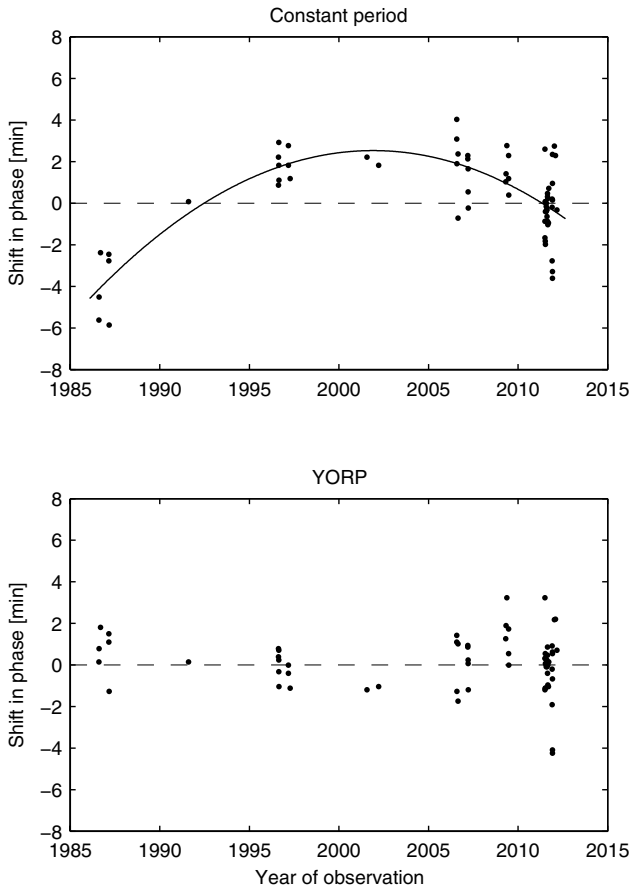

Fig. 4. Shift in phase between the observed and modeled lightcurves for the constant-period model (*top*) and the model with YORP (*bottom*), $\upsilon = 1.2 \times 10^{-8}$ rad d^{-2}. The points in the *top panel* are fitted with a quadratic function.

2.3. (2100) Ra-Shalom

The UAPC contains lightcurves of Ra-Shalom from 1978 to 1997 obtained by Harris et al. (1992), Ostro et al. (1984), and Pravec et al. (1998). Kaasalainen et al. (2004) used this dataset, together with a few Ondřejov lightcurves from Ra-Shalom's apparition in 2000, to construct a pole and shape model. Because their data set was limited, they flagged their model to be only a preliminary attempt. Indeed, it is significantly different from the new one we present here, because we used additional photometry from 2003 and 2009 listed in Table 3. The derived shape model is shown in Fig. 8 and the fit to selected lightcurves in Fig. 9. While our model is an improvement, it is still not perfect. In particular, the pole direction is still not well constrained, with the formally best solution at $\lambda = 313°$ and $\beta = -45°$. The statistically admissible solutions cover an irregularly-shaped region on the sky as shown in Fig. 10. The contour corresponds to solutions with an 8% higher value of χ^2 than the minimum. Because the number of degrees of freedom is $\nu \simeq 2300$, the 8% increase corresponds to 3σ in the χ^2 distribution (see the footnote on page 3). The statistical weight of prograde-rotating spin solutions is negligible. All solutions in our formal 3σ region correspond to a retrograde sense of rotation for Ra-Shalom. That our zone of admissible pole solutions is a subset of a similar zone presented by Shepard et al. (2008) (see Fig. 7 in this reference), who carefully analyzed radar and other wavelength observations of Ra-Shalom, gives us an increased confidence in our solution. The sidereal rotation period is $P = 19.8201 \pm 0.0004$ h. No deviation from uniform rotation has been detected so far. The maximum value of the change in the rotation rate was estimated to $-4 \times 10^{-8} < \upsilon < 2 \times 10^{-8}$ rad d^{-2}.

3. Discussion

Two of our pole solutions, namely those of Eger and Cerberus, correspond to a near-extreme obliquity value: we have $\varepsilon \simeq 176°$ for Eger and $\varepsilon \simeq 178°$ for Cerberus. Both values have about a 10° uncertainty in realistic terms. While the formal obliquity value of the best-fit solution for Ra-Shalom is ≃144°, Fig. 10 indicates that basically all retrograde values are possible, including the value near 180° (note location of the orbital south pole in this figure), so at least two, possibly even all three, of our asteroids belong to the most populated class of near-Earth objects, those with an extremely high value of obliquity (La Spina et al. 2004; Kryszczyńska et al. 2007).

The retrograde sense of rotation for all our targets is consistent with an independent estimate of the Yarkovsky acceleration in their orbits. Chesley et al. (2008) attempted to estimate Yarkovsky effect in orbits of all near-Earth asteroids by including a formal along-track acceleration in their orbital fit and by estimating the related parameter da/dt, namely a secular change in the orbital semimajor axis a (see also Nugent et al. 2012). Because the diurnal variant of the Yarkovsky effect is dominant in the dynamics of near-Earth asteroids, a positive/negative value for da/dt value implies a prograde/retrograde sense of rotation of the asteroid (see, for example, Bottke et al. 2006). In the case of all three asteroids discussed in this paper, Chesley et al. (2008) give a negative best-fit value for da/dt, thus requiring a retrograde sense of their rotation. This is especially important for Ra-Shalom, for which the previous solution by Kaasalainen et al. (2004) implies prograde rotation, while here we find a retrograde solution.

3.1. Theoretical YORP strengths

We now proceed with a theoretical estimation of the YORP strength for our targets. In a sense, this is merely a consistency check that the observed secular increase in the rotation rate υ (in the case of Eger) can be interpreted as a YORP effect detection. This is because a number of parameters, such as exact size, bulk density, and surface conductivity, are only weakly constrained, and even knowledge of the large-scale surface-shape features may still not be enough for precise YORP computations (Statler 2009; Breiter et al. 2009; Rozitis & Green 2012; Golubov & Krugly 2012).

(3103) Eger. We used the model of Breiter & Vokrouhlický (2011) to estimate the YORP value of υ for our shape of Eger. We considered parameters of the Hapke scattering model of the E-type asteroids (Breiter & Vokrouhlický 2011) and varied the value of geometric albedo between 0.4 and 0.6. This is because the latest solutions presented by Trilling et al. (2010) and Harris et al. (2011) give a little larger size of $D \simeq 1.78$ km for a lower albedo value of $p \simeq 0.39$, while previous solutions had smaller sizes of $D \simeq 1.5$ km and larger albedo (Benner et al. 1997). We also varied the bulk density value between 2.5 and 3 g/cm^3 and assumed surface thermal conductivity of 0.01 W/m/K. However, as was shown by Breiter et al. (2010), for 1D thermal models, the resulting YORP value of υ does not depend on the value of conductivity. We scaled the lightcurve-inversion shape model (Fig. 2) to have the same volume as a sphere of 1.78 km size. A straightforward use of our model gives values for υ between 4.1×10^{-8} rad d^{-2} and 8.3×10^{-8} rad d^{-2}. However, we

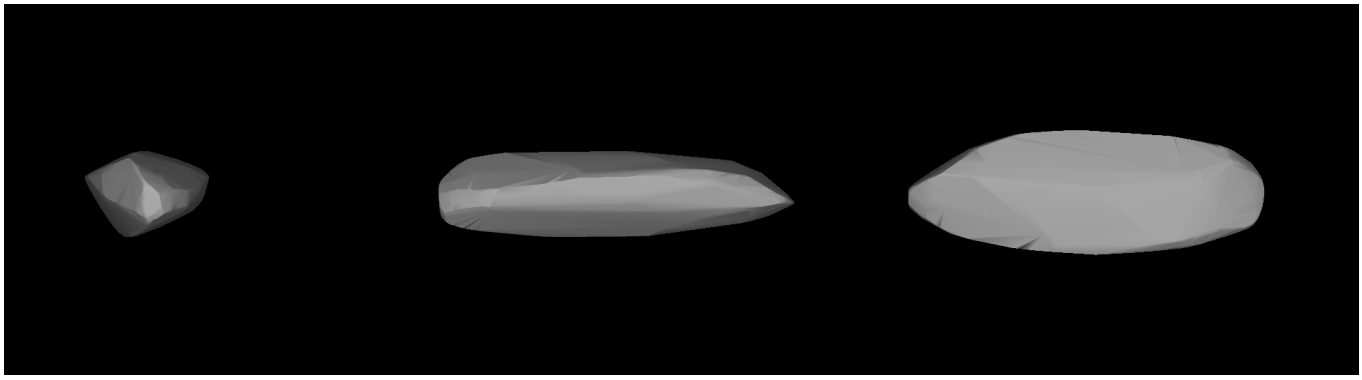

Fig. 5. Convex shape model of Cerberus shown from equatorial level (*left, center*) and pole-on (*right*).

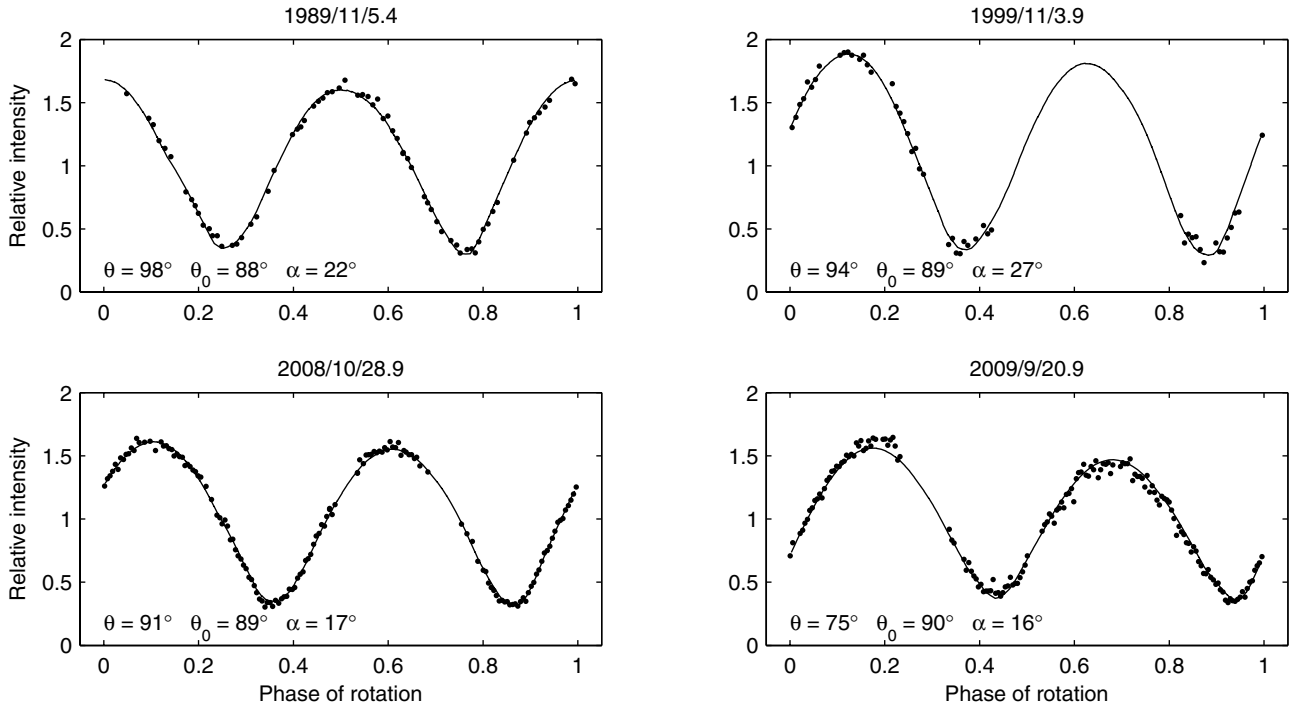

Fig. 6. Examples of Cerberus' lightcurves fitted with synthetic ones based on the convex shape model. The viewing and illumination geometry is given by the aspect angle θ, the solar aspect angle θ_0, and the solar phase angle α.

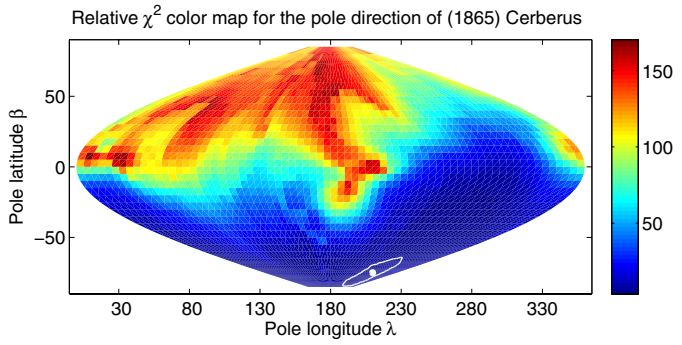

Fig. 7. Statistical quality of Cerberus pole solutions given in sinusoidal projection of the sky in ecliptic coordinates. The grade of shading and the scale bar on the right indicate the χ^2 of the fit divided by the number of data points. The formally best-fit case with $\lambda = 298°$ and $\beta = -72°$ is marked with a full circle. The solid line shows the contour with the χ^2 value 10% higher than the minimum value of the best-fit solution. It represents our region of admissible solutions.

note that the lightcurve inversion technique does not a priori constrain the axes of the shape model to coincide with the principal axes of the inertia tensor. Obviously a large difference would signal a suspicious model. Assuming a homogeneous density distribution, we find there is about a 5° tilt between the z-axes of the two systems, which is too small an angle for the correction to be determined by photometry analysis. Assuming thus that the body rotates about its shortest axis of the inertia tensor, and preserving the body's shape, we now obtain υ values between 4.4×10^{-8} rad d^{-2} and 7.5×10^{-8} rad d^{-2}. Compared to the observed value $\upsilon = (1.4 \pm 0.6) \times 10^{-8}$ rad d^{-2}, our estimates are a factor of three to six times higher, a situation similar to the case of (54509) YORP (Lowry et al. 2007; Taylor et al. 2007). In the latter case, the lightcurve and radar data were not able to sample signal from about 30% of the surface, which was one of the sources of the difference between the observed and computed υ values. In the case of Eger, we only have knowledge of the large-scale features of the asteroid shape – the lightcurve data do not give any information about the small-scale irregularities of the shape and the effects of thermal beaming. We believe this is the main source of the difference between the observed value for υ and the one computed from YORP theory. Indeed, Benner et al. (1997) provide a hint from the analysis of the radar ranging to

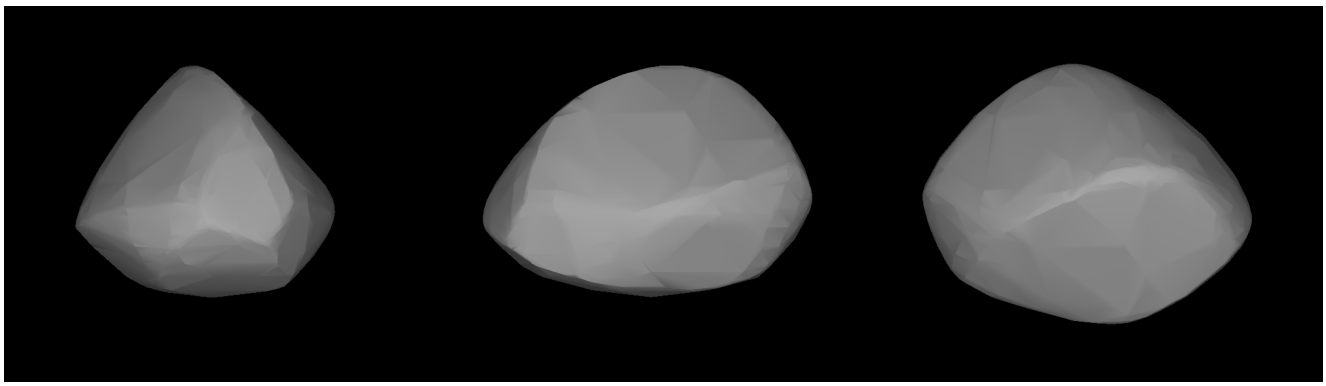

Fig. 8. Convex shape model of Ra-Shalom shown from equatorial level (*left, center*) and pole-on (*right*).

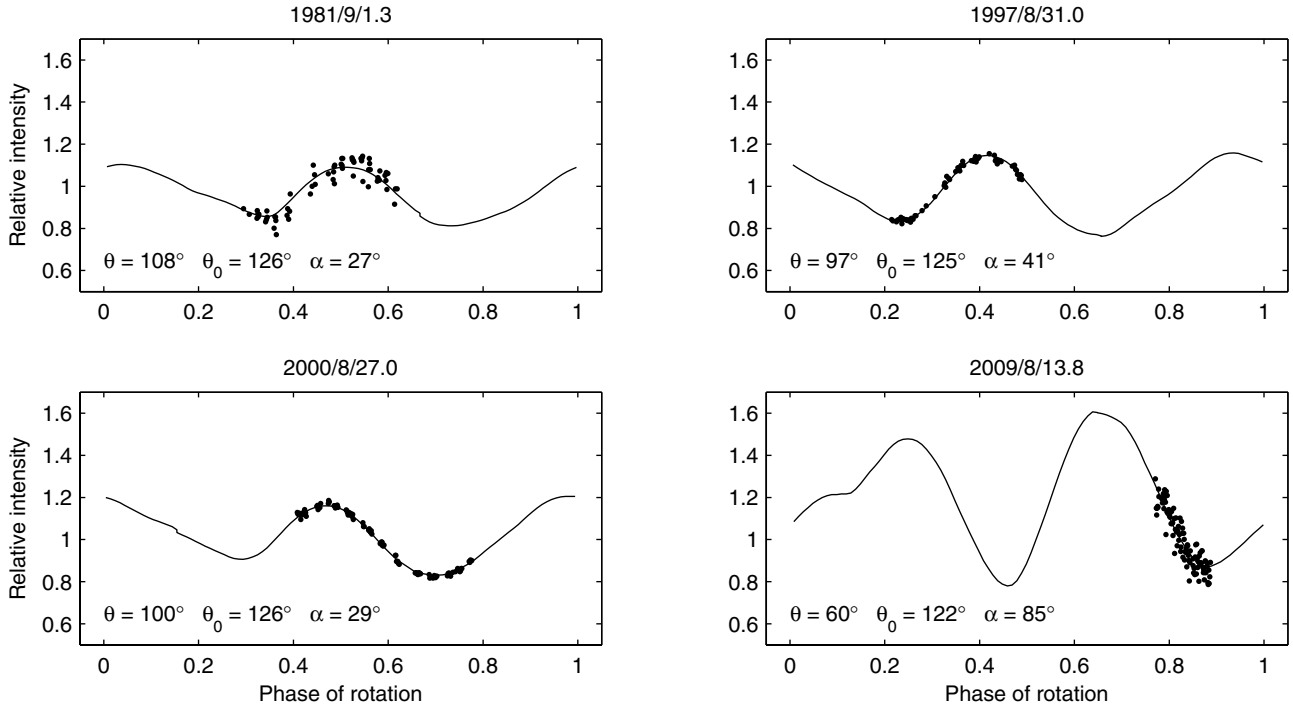

Fig. 9. Examples of Ra-Shalom's lightcurves fitted with synthetic ones based on the convex shape model. The viewing and illumination geometry is given by the aspect angle θ, the solar aspect angle θ_0, and the solar phase angle α.

Eger that these small-scale features might actually be very significant.

(1865) Cerberus. The shape of Cerberus derived above suggests that even its large-scale structures were not accurately determined by our convex model. Obviously, we could have tried to resolve some nonconvexities in the model, too, but the currently available set of the photometric observations is not large enough to derive a unique model. We thus consider our convex model as the current, but certainly preliminary, state-of-the-art representation of its shape. We used the mean Hapke parameters of the S-type asteroids in this case (Breiter & Vokrouhlický 2011) and scaled the shape model to have the same volume as a sphere with the diameter of 1.6 km (Mainzer et al. 2011). We also varied the geometric albedo value between 0.1 and 0.2. The bulk density was 2.5 g/cm^3. With these values, we obtained the YORP-predicted $\upsilon \simeq 2 \times 10^{-8}$ rad d^{-2}, which was two to three times larger than the conservative bound we obtained from the observations in Sect. 2.2. Obviously, this difference may be due to a number of unconstrained factors, the inaccurate shape model first of all. The key to further analysis of the Cerberus case

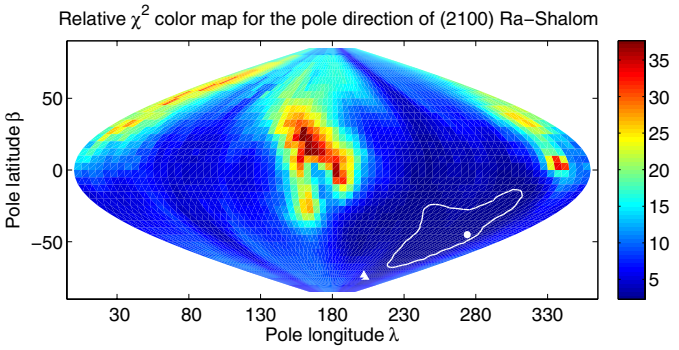

Fig. 10. Statistical quality of Ra-Shalom pole solutions given in sinusoidal projection of the sky in ecliptic coordinates. The grade of shading and the scale bar on the right indicate the χ^2 of the fit divided by the number of data points. The formally best-fit case with $\lambda = 313°$ and $\beta = -45°$ is marked with a full circle. The solid line shows the contour with the χ^2 value 8% higher than the minimum value of the best-fit solution. It represents our region of admissible solutions. The pole of the orbital plane corresponding to 180° obliquity, shown by the triangle, is located close to this zone.

consists in obtaining additional observations, which are needed not only for possible future detection of the YORP effect but also for improving the shape model itself. A good opportunity occurred in October 2016, when this asteroid could be observed at large phase angles, and from September to November 2017.

It is interesting to note that the photometric data are consistent with a highly nonconvex, bilobed model, but they might also be fitted with a very close binary system. Using the analysis performed by Bellerose & Scheeres (2008) or Scheeres (2009), we note there are possible stable equilibria of two ellipsoids (or an ellipsoid and a sphere) with reasonable density values between 1 and 3 g/cm^3 that could match a synchronously rotating system with Cerberus' observed period of ~6.81 h and small separations.

(2100) Ra-Shalom. In the case of Ra-Shalom, we scaled our shape model to be equivalent to a sphere of ~2.3 km size (Shepard et al. 2008; Trilling et al. 2010; Harris et al. 2011) and took a geometric albedo of 0.1 (Ra-Shalom is an S-type asteroid). We used a bulk density of 2 g/cm^3 and our best-fit formal solution for the pole. The formal obliquity value $\varepsilon \simeq 144°$ tends to minimize the computed effect because YORP has been found to have a node $\upsilon \simeq 0$ near $\varepsilon \simeq 125°$ for generic shapes (Čapek & Vokrouhlický 2004; Vokrouhlický & Čapek 2002). With these parameter values, we obtained $\upsilon \simeq -6 \times 10^{-8}$ rad d^{-2}, a little larger than its upper bound derived from the lightcurve observations (Sect. 2.3). For this value, we had a negative value of $\upsilon = \mathrm{d}\omega/\mathrm{d}t$, implying that, for a given shape model, YORP should decelerate the rotation rate of the body. This conclusion would seem consistent with the rather long rotation period of ≃19.82 h of this asteroid. However, we should point out the large current uncertainty in the obliquity of the pole solution (Fig. 10). For instance, sampling the uncertainty region by pole positions along the meridian of the formally best solution (i.e., keeping longitude equal to 313°) and taking latitude values from −10° to −75°, we obtain υ values from 2×10^{-8} rad d^{-2} to -9×10^{-8} rad d^{-2}. As expected, for obliquities below ~125°, we obtain a positive value for υ; however, for obliquities greater than ~125°, which includes the formally best-fit solution, the value for υ is negative. While positive υ values still cannot be excluded, the majority of pole solutions in the uncertainty interval shown in Fig. 10 correspond to negative υ values. As a result, if carefully observed during the next few years (notably in late summer 2013 and 2016), Ra-Shalom might become the first asteroid for which YORP will be found to decrease the rotation rate.

Acknowledgements. We thank an anonymous referee for helpful comments that improved the final version. The work of J.Ď. and D.V. was supported by grants P209/10/0537, 205/08/0064, and P209/12/0229 of the Czech Science Foundation and by the Research Program MSM0021620860 of the Ministry of Education. The work of S.B. was supported by the Polish National Science Center – grant NN 203404139. The work of M.K. was supported by the Academy of Finland. The work of P.P. was supported by grant P209/12/0229 of the Czech Science Foundation. D.P. is grateful to the AXA research fund and to the continuous support from the Wise Observatory staff. F.M. was supported by the National Science Foundation under award number AAG-08077468. G.S. was supported by Hungarian OTKA Grants K-104607, MB08C 81013, a "Lendulet" Programme and a Bolyai Research Fellowship of the Hungarian Academy of Sciences.

References

Bellerose, J., & Scheeres, D. J. 2008, Celest. Mech. Dyn. Astron., 100, 63
Benner, L. A. M., Ostro, S. J., Giorgini, J. D., et al. 1997, Icarus, 130, 296
Bottke, Jr., W. F., Vokrouhlický, D., Rubincam, D. P., & Nesvorný, D. 2006, Ann. Rev. Earth Planet. Sci., 34, 157
Breiter, S., & Vokrouhlický, D. 2011, MNRAS, 410, 2807
Breiter, S., Bartczak, P., Czekaj, M., Oczujda, B., & Vokrouhlický, D. 2009, A&A, 507, 1073
Breiter, S., Bartczak, P., & Czekaj, M. 2010, MNRAS, 408, 1576
Čapek, D., & Vokrouhlický, D. 2004, Icarus, 172, 526
Chesley, S. R., Vokrouhlický, D., Ostro, S. J., et al. 2008, LPI Contributions, 1405, 8330
de Sanctis, M. C., Barucci, M. A., Angeli, C. A., et al. 1994, Planet. Space Sci., 42, 859
Ďurech, J., & Kaasalainen, M. 2003, A&A, 404, 709
Ďurech, J., Vokrouhlický, D., Kaasalainen, M., et al. 2008, A&A, 488, 345
Ďurech, J., Sidorin, V., & Kaasalainen, M. 2010, A&A, 513, A46
Golubov, O., & Krugly, Y. N. 2012, ApJ, 752, L11
Harris, A. W., & Young, J. W. 1989, Icarus, 81, 314
Harris, A. W., Young, J. W., Dockweiler, T., et al. 1992, Icarus, 95, 115
Harris, A. W., Mommert, M., Hora, J. L., et al. 2011, AJ, 141, 75
Kaasalainen, M., & Torppa, J. 2001, Icarus, 153, 24
Kaasalainen, M., & Viikinkoski, M. 2012, A&A, 543, A97
Kaasalainen, M., Torppa, J., & Muinonen, K. 2001, Icarus, 153, 37
Kaasalainen, M., Torppa, J., & Piironen, J. 2002, Icarus, 159, 369
Kaasalainen, M., Pravec, P., Krugly, Y. N., et al. 2004, Icarus, 167, 178
Kaasalainen, M., Ďurech, J., Warner, B. D., Krugly, Y. N., & Gaftonyuk, N. M. 2007, Nature, 446, 420
Kaasalainen, S., Piironen, J., Kaasalainen, M., et al. 2003, Icarus, 161, 34
Krugly, Y. N., Belskaya, I. N., Shevchenko, V. G., et al. 2002, Icarus, 158, 294
Kryszczyńska, A., La Spina, A., Paolicchi, P., et al. 2007, Icarus, 192, 223
La Spina, A., Paolicchi, P., Kryszczyńska, A., & Pravec, P. 2004, Nature, 428, 400
Lagerkvist, C.-I., Piironen, J., & Erikson, A. 2001, Asteroid photometric catalogue, fifth update (Uppsala Astronomical Observatory)
Lowry, S. C., Fitzsimmons, A., Pravec, P., et al. 2007, Science, 316, 272
Mainzer, A., Grav, T., Bauer, J., et al. 2011, ApJ, 743, 156
Milani, A., Carpino, M., Hahn, G., & Nobili, A. M. 1989, Icarus, 78, 212
Nugent, C. R., Margot, J. L., Chesley, S. R., & Vokrouhlický, D. 2012, AJ, 144, 60
Ostro, S. J., Harris, A. W., Campbell, D. B., Shapiro, I. I., & Young, J. W. 1984, Icarus, 60, 391
Polishook, D., & Brosch, N. 2008, Icarus, 194, 111
Polishook, D., & Brosch, N. 2009, Icarus, 199, 319
Pravec, P., & Harris, A. W. 2007, Icarus, 190, 250
Pravec, P., Wolf, M., & Šarounová, L. 1998, Icarus, 136, 124
Pravec, P., Harris, A. W., Vokrouhlický, D., et al. 2008, Icarus, 197, 497
Pravec, P., Vokrouhlický, D., Polishook, D., et al. 2010, Nature, 466, 1085
Rozitis, B., & Green, S. F. 2012, MNRAS, 423, 367
Sárneczky, K., Szabó, G., & Kiss, L. L. 1999, A&AS, 137, 363
Scheeres, D. J. 2007, Icarus, 189, 370
Scheeres, D. J. 2009, Celest. Mech. Dyn. Astron., 104, 103
Scheeres, D. J., & Gaskell, R. W. 2008, Icarus, 198, 125
Shepard, M. K., Clark, B. E., Nolan, M. C., et al. 2008, Icarus, 193, 20
Statler, T. S. 2009, Icarus, 202, 502
Szabó, G. M., Csák, B., Sárneczky, K., & Kiss, L. L. 2001, A&A, 375, 285
Taylor, P. A., Margot, J.-L., Vokrouhlický, D., et al. 2007, Science, 316, 274
Trilling, D. E., Mueller, M., Hora, J. L., et al. 2010, AJ, 140, 770
Velichko, F. P., Krugly, Y. N., & Chiorny, V. G. 1992, Astronomicheskij Tsirkulyar, 1553, 37
Vokrouhlický, D., & Čapek, D. 2002, Icarus, 159, 449
Vokrouhlický, D., & Nesvorný, D. 2008, AJ, 136, 280
Vokrouhlický, D., Nesvorný, D., & Bottke, W. F. 2003, Nature, 425, 147
Vokrouhlický, D., Brož, M., Bottke, W. F., Nesvorný, D., & Morbidelli, A. 2006, Icarus, 182, 118
Walsh, K. J., Richardson, D. C., & Michel, P. 2008, Nature, 454, 188
Wisniewski, W. Z. 1987, Icarus, 70, 566
Wisniewski, W. Z. 1991, Icarus, 90, 117
Wisniewski, W. Z., Michalowski, T. M., Harris, A. W., & McMillan, R. S. 1997, Icarus, 126, 395

Table 1. Aspect data for new observations of Eger.

Date	r [AU]	Δ [AU]	α [deg]	λ [deg]	β [deg]	Obs.
1996 07 20.0	1.156	0.194	40.3	343.6	12.7	Si
1997 02 05.0	1.459	0.483	9.8	145.9	11.0	Kh
2001 06 24.9	1.294	0.422	41.3	326.1	26.8	Si
2002 02 16.8	1.515	0.544	11.8	139.0	15.9	On
2006 06 28.9	1.269	0.388	42.3	330.3	25.0	Kh
2006 06 30.0	1.263	0.378	42.3	330.9	24.8	Kh
2006 06 30.9	1.258	0.368	42.4	331.5	24.5	Kh
2006 07 26.0	1.122	0.163	46.2	355.6	1.1	Kh
2007 02 10.3	1.486	0.510	9.4	144.7	13.8	SRO
2007 02 12.3	1.496	0.520	9.6	143.4	14.7	SRO
2007 02 17.3	1.520	0.550	11.8	140.3	16.5	GM
2007 02 19.0	1.527	0.560	12.7	139.5	17.0	Si
2009 03 22.0	1.902	1.113	24.1	221.3	35.4	W1
2009 03 29.0	1.903	1.076	22.6	219.3	37.3	W1
2009 04 15.9	1.898	1.023	20.3	211.4	40.6	Si
2009 05 17.9	1.867	1.076	25.7	196.9	38.3	W1
2009 05 18.8	1.866	1.080	25.9	196.6	38.1	W1
2009 05 24.8	1.857	1.107	27.5	195.3	36.8	W1
2011 06 01.0	1.410	0.688	42.3	317.0	26.4	Ab
2011 06 04.0	1.395	0.654	42.6	318.7	26.4	On
2011 06 04.0	1.394	0.654	42.6	318.7	26.4	W2
2011 06 05.0	1.390	0.644	42.6	319.2	26.4	Li
2011 06 05.0	1.389	0.643	42.6	319.2	26.4	On
2011 06 05.9	1.384	0.633	42.7	319.8	26.3	W2
2011 06 06.0	1.384	0.632	42.7	319.8	26.3	On
2011 06 09.0	1.369	0.600	42.9	321.4	26.2	Li
2011 06 10.0	1.363	0.589	43.0	322.0	26.2	Ab
2011 06 10.9	1.358	0.579	43.1	322.6	26.1	W2
2011 06 25.0	1.282	0.434	44.1	331.2	24.2	On
2011 06 27.0	1.272	0.414	44.2	332.5	23.7	On
2011 06 28.0	1.266	0.404	44.3	333.3	23.5	On
2011 07 02.3	1.242	0.363	44.7	336.4	22.0	On
2011 07 08.0	1.211	0.311	45.4	341.2	19.3	W2
2011 07 12.9	1.184	0.269	46.2	345.8	15.8	Kh
2011 07 22.9	1.130	0.196	50.4	358.4	3.7	Kt
2011 07 22.9	1.130	0.196	50.4	358.5	3.7	Ab
2011 07 23.0	1.129	0.196	50.5	358.6	3.5	On
2011 07 25.0	1.119	0.185	52.0	1.8	0.1	Ab
2011 07 27.0	1.108	0.175	54.0	5.4	−3.9	Ab
2011 07 27.3	1.106	0.173	54.4	6.1	−4.7	On
2011 08 13.4	1.023	0.171	82.0	52.4	−42.8	On
2011 08 14.4	1.018	0.175	83.4	55.6	−44.1	On
2011 10 25.3	0.953	0.581	76.6	147.1	−33.5	PR
2011 10 26.3	0.956	0.584	76.2	147.7	−33.2	PR
2011 10 27.3	0.959	0.587	75.8	148.2	−32.8	PR
2011 10 29.3	0.966	0.592	74.9	149.3	−32.2	PR
2011 10 30.3	0.970	0.594	74.5	149.8	−31.8	PR
2011 11 01.3	0.977	0.598	73.7	150.8	−31.1	PR
2011 11 02.3	0.981	0.600	73.3	151.3	−30.8	PR
2011 11 03.3	0.985	0.602	72.9	151.8	−30.4	PR
2011 12 09.1	1.160	0.587	58.1	164.9	−17.8	W2
2011 12 30.0	1.274	0.530	46.1	166.4	−8.7	Ab
2012 01 30.3	1.439	0.488	17.6	154.4	8.9	PR

Notes. The table lists the asteroid's distance from the Sun r and from the Earth Δ, the solar phase angle α, the geocentric ecliptic coordinates of the asteroid (λ,β), and the observatory (W1 – Wise Observatory, 1 m; W2 – Wise Observatory, 46 cm; Kh – Kharkiv Observatory, 70 cm; Si – Simeiz, Crimean Astronomical Observatory, 1 m; GM – Goat Mountain Astronomical Research Station, 35 cm; SRO – Sonoita Research Observatory, 35 cm; On – Ondřejov Observatory, 65 cm; Li – Lisnyky, Kiev University Observatory, 70 cm; Ab – Abastumani Astrophysical Observatory, 1.25 m; Ki – Kitab Observatory, 40 cm; PR – PROMPT, 45 cm).

Table 2. Aspect data for new observations of Cerberus.

Date	r [AU]	Δ [AU]	α [deg]	λ [deg]	β [deg]	Obs.
1999 11 03.9	1.432	0.529	27.3	359.9	4.7	On
1999 11 04.9	1.428	0.532	28.2	359.3	4.3	On
2008 09 01.9	1.574	0.822	34.4	40.4	14.4	Ma
2008 09 02.9	1.573	0.811	34.0	40.4	14.4	Ma
2008 09 24.9	1.535	0.606	22.6	35.8	13.4	Si
2008 09 30.6	1.521	0.562	18.1	33.0	12.7	Le
2008 10 20.9	1.455	0.467	8.5	17.8	7.5	On
2008 10 28.9	1.422	0.459	17.3	10.9	4.5	Kh
2008 10 29.3	1.420	0.459	17.8	10.6	4.3	Li
2008 11 03.8	1.396	0.463	24.3	6.3	2.1	On
2009 09 19.9	1.583	0.617	16.0	355.6	25.7	Wi
2009 09 20.9	1.583	0.617	15.9	354.9	25.5	Wi
2009 10 15.9	1.575	0.703	26.5	340.4	17.1	HP
2009 10 18.8	1.572	0.721	28.2	339.4	16.0	Si

Notes. The table lists the asteroid's distance from the Sun r and from the Earth Δ, the solar phase angle α, the geocentric ecliptic coordinates of the asteroid (λ,β), and the observatory (On – Ondřejov Observatory, 65 cm; Kh – Kharkiv Observatory, 70 cm; Si – Simeiz, Crimean Astronomical Observatory, 1 m; Le – Leura Observatory, 36 cm; Ma – Maidanak Observatory, 1 m; Wi – Wise Observatory, 1 m; HP – Observatoire de Haute-Provence, 1.2 m; Li – Lick Observatory, 1 m).

Table 3. Aspect data for new observations of Ra-Shalom.

Date	r [AU]	Δ [AU]	α [deg]	λ [deg]	β [deg]	Obs.
2003 08 06.9	1.083	0.188	63.9	8.0	61.0	Kh
2003 08 07.0	1.083	0.188	63.7	7.7	61.0	Kh
2003 08 24.0	1.147	0.180	37.9	316.3	42.3	Kh
2003 08 25.0	1.150	0.182	37.1	314.6	40.6	Si
2003 08 26.0	1.153	0.184	36.5	313.1	38.9	Si
2003 08 27.0	1.156	0.187	36.0	311.6	37.2	Si
2003 08 27.9	1.158	0.189	35.7	310.4	35.6	Si
2003 08 28.8	1.160	0.192	35.4	309.3	34.1	Si
2003 08 29.9	1.163	0.196	35.3	308.0	32.3	Si
2003 08 30.9	1.166	0.199	35.3	307.0	30.7	Si
2003 09 01.0	1.168	0.203	35.5	305.9	28.9	On
2003 09 03.0	1.172	0.212	36.0	304.3	26.0	On
2003 09 05.9	1.178	0.225	37.3	302.4	21.9	On
2003 09 06.9	1.180	0.230	37.9	301.8	20.5	On
2003 09 14.9	1.190	0.275	42.8	299.0	11.8	On
2003 09 15.8	1.191	0.281	43.4	298.8	11.0	On
2003 09 16.8	1.192	0.287	44.0	298.7	10.1	On
2003 09 17.8	1.193	0.293	44.6	298.5	9.2	On
2009 08 13.8	0.980	0.362	84.8	212.2	33.3	W2
2009 08 13.8	0.980	0.362	84.8	212.2	33.3	W1
2009 08 14.8	0.986	0.363	83.8	214.4	33.0	W2
2009 08 16.8	0.998	0.365	81.8	218.9	32.2	W1
2009 08 17.8	1.004	0.367	80.8	221.0	31.7	W1
2009 08 23.8	1.039	0.383	75.2	233.1	28.5	Kh
2009 09 19.7	1.150	0.541	60.8	268.0	12.7	W1
2009 09 20.7	1.153	0.548	60.5	268.9	12.2	W1
2009 09 21.7	1.156	0.556	60.3	269.7	11.7	W1

Notes. The table lists the asteroid's distance from the Sun r and from the Earth Δ, the solar phase angle α, the geocentric ecliptic coordinates of the asteroid (λ,β), and the observatory (Si – Simeiz, Crimean Astronomical Observatory, 1 m; W1 – Wise Observatory, 1 m; W2 – Wise Observatory, 46 cm; Kh – Kharkiv Observatory, 70 cm; On – Ondřejov Observatory, 65 cm).